



Kinetics of the Reaction of Ferrous Ions with Hydroxyl Radicals in the Temperature Range 25-300 °C

Journal:	Physical Chemistry Chemical Physics	
Manuscript ID	CP-ART-08-2023-003819.R3	
Article Type:	Paper	
Date Submitted by the Author:	02-Jan-2024	
Complete List of Authors:	Barr, Logan; Canadian Nuclear Laboratories, Reactor Chemistry and Corrosion Conrad, Jacy K; Idaho National Laboratory, McGregor, Christine; Canadian Nuclear Laboratories, Reactor Chemistry and Corrosion Perron, Randy; Canadian Nuclear Laboratories, Radiobiology and Health Yakabuskie, Pamela; Canadian Nuclear Laboratories, Reactor Chemistry and Corrosion Stuart, Craig; Canadian Nuclear Laboratories, Reactor Chemistry and Corrosion Branch	

SCHOLARONE™ Manuscripts

ARTICLE

Kinetics of the Reaction of Ferrous Ions with Hydroxyl Radicals in the Temperature Range 25-300 °C

Received 00th January 20xx, Accepted 00th January 20xx

DOI: 10.1039/x0xx000000x

Logan Barr, *a Jacy K. Conrad^b, Christine McGregor^a, Randy Perron^a, Pamela A. Yakabuskie^a and Craig R. Stuart^a

The kinetics and mechanism of the reaction between OH radicals and ferrous ions in the temperature range 25-300 °C were studied using pulse radiolysis. At temperatures < 150 °C the rate of reaction is essentially independent of temperature, while at temperatures > 150 °C the activation energy is 45.8 ± 3.0 kJ mol⁻¹. The change in activation energy is attributed to a change in the dominant mechanism from hydrogen atom transfer (HAT) to dissociative ligand interchange. The kinetic isotope effect (KIE) was measured by repeating experiments in heavy water. A value of 2.9 was measured at room temperature where HAT is the dominant mechanism. The KIE decreases to zero at temperatures > 150 °C as ligand interchange becomes dominant and the O-H bond is no longer involved in the reaction.

Introduction

The corrosion and dissolution of steels is a concern when considering reactor lifetimes and activity transport because they are a construction material in the primary side heat transport systems of nuclear reactors. Corrosion of steel materials leads to the dissolution of iron ions into the aqueous coolant¹. When making predictions of the behaviour of iron species in reactors, the usual approach is based on solubility measurements determined in the absence of radiation^{2,3}. Under ionising radiation, radiolysis of water produces a number of highly reactive oxidising and reducing species, which react with dissolved metal ions and alter the behaviour of dissolved species⁴.

Iron speciation and solubility is often considered from a thermodynamic perspective, without accounting for the effect of water radiolysis on the oxidation state of iron in solution. Modelling of radiation chemistry relies on the availability of a comprehensive set of rate constants. For high temperature systems, the activation energies of the reactions are also necessary to accurately model the chemistry⁵. While the temperature dependences of many water radiolysis products are well established, there are many species for which available data is sparse.

Iron is a major component of many reactors, however, the high temperature radiation chemistry of soluble iron species is not well understood. There are few studies available in literature addressing the rates of reactions of iron species with OH radicals^{6,7}, and even fewer that consider the reaction temperature dependences.^{8,9}

Radiolysis of water results in the splitting of water molecules to form radical and molecular species (R1). These water radiolysis products participate in redox reactions with one another and other aqueous species. Hydrated electrons (e_{aq}) are strongly reducing, while hydroxyl radicals (*OH) are strongly oxidising.¹⁰

$$H_2O \xrightarrow{\text{Radiation}} e_{\text{aq}}^-, H, OH, HO_2/O_2^-, H_2O_2, H_2$$
 (R1)

Oxidation of ferrous ions produces less soluble ferric ions¹¹, and is a potentially important process in the deposition of corrosion products in reactor heat transport systems. The most oxidising species formed during water radiolysis is the hydroxyl radical, which reacts with Fe^{2+} to form $Fe(OH)^{2+}$ through reaction R2.

$$[Fe(H_2O)_6]^{2+} + OH \longrightarrow [Fe(H_2O)_5(OH)]^{2+} + H_2O$$
 (R2)

Oxidation of iron in solution by *OH is a potential driving force for changes to the solubility and speciation of iron present in an irradiated environment.

The kinetics and mechanism of R2 have been studied previously at room temperature by a number of groups⁶⁻⁹ and only a single study of the temperature dependence exists at high temperature⁹ (> 150 °C). Jayson et al. measured the rate constant over a modest temperature range of 17 - 67 °C and reported a room temperature value of $(2.3 \pm 0.2) \times 10^8 \,\mathrm{M}^{-1} \,\mathrm{s}^{-1}$, which was unaffected by increasing temperature⁹. They also performed the experiments in both light and heavy water, reporting a slower rate of reaction in heavy water, $(9.7 \pm 1.0) \times 10^7 \,\mathrm{M}^{-1} \,\mathrm{s}^{-1}$ as a result of the kinetic isotope effect (KIE). The mechanism of the reaction was stated as an electron transfer, with the observed KIE attributed to differences in the free energy of hydration between light and heavy water. However, Stuglik and Zagorsky⁶ performed tests at room temperature in neutral solution, and performed modelling of the two possible mechanisms based on the intermediate

^{a.} Reactor Chemistry and Corrosion, Canadian Nuclear Laboratories, 286 Plant Road, Chalk River, Ontario, Canada, K0J1J0.

b. Center for Radiation Chemistry Research, Idaho National Laboratory, 1955 N. Fremont Ave., Idaho Falls, ID, 83415, USA.

expected. The modelling showed a good fit for a single step hydrogen abstraction, and a poor fit for electron transfer, which allowed outer sphere charge transfer to be discounted as a possible mechanism at room temperature. Stuglik and Zagorsky discounted the possibility of a ligand interchange mechanism on the basis that the limiting rate of water exchange¹² (4.4 x 10⁶ M⁻¹ s⁻¹) is two orders of magnitude slower than the observed rate constant of 3.2 x 108 M⁻¹ s⁻¹. By elimination of other possible mechanisms, it was concluded that at room temperature, R2 proceeds via a hydrogen atom abstraction mechanism. A single study addressed the temperature dependence of R2 up to 220 °C in acidic solution9. Contrary to the findings of Jayson et al., the temperature dependence of the reaction was reported to conform to a typical Arrhenius relationship, exhibiting an activation energy of 9 kJ mol⁻¹ and a room temperature rate constant of $4.3 \times 10^8 \pm 0.6 \text{ M}^{-1} \text{ s}^{-1}$. This disagreement surrounding the temperature dependence of the reaction and its potential importance in understanding reactor coolant chemistry prompted further investigation into the reaction at elevated temperatures.

Experimental

Materials

Solutions were prepared from Millipore deionised water (resistivity > 18 M Ω cm⁻¹) and iron (II) sulphate (99.5%) in concentrations of 1.4, 5.0, and 9.3 x 10^{-4} M at pH 3. The pH of the solutions was adjusted using sulphuric acid (93 – 98 % trace metal grade) to ensure Fe²⁺ remained in solution as the hexaaqua ion² across the temperature range. Solutions were bubbled with N₂O for at least 30 minutes to ensure removal of oxygen and saturation of the solution with N₂O to scavenge reducing radicals (eaq and H*), converting them to *OH through reactions (R3-R5)¹³.

$$N_2O + e_{aq}^- \longrightarrow O^{\bullet -} + N_2$$
 (R3)

$$0^{\bullet-} + H^+ \longrightarrow {}^{\bullet}OH$$
 (R4)

$$N_2O + H^{\bullet} \longrightarrow {}^{\bullet}OH + N_2$$
 (R5)

In a saturated solution of N_2O R3 will outcompete other hydrated electron reactions, including reaction with the ferrous ion¹⁴. The O^{\bullet} radical will be rapidly protonated to form ${}^{\bullet}OH$ at pH 3.

Heavy water (99.9% D) was purchased from Sigma Aldrich and distilled with potassium permanganate and sodium bicarbonate (99.5%) purchased from Fisher Scientific.

Iron concentrations in solution were determined using the phenanthroline method, in which an excess of 1,10-phenanthroline (Aldrich, > 99 %) is added to the solution to form a complex with Fe $^{2+}$ ions, resulting in a strong absorbance (ϵ = 11,100 M^{-1} cm $^{-1}$) at 508 nm. 15 Total iron was measured by reduction of all iron in solution using ascorbic acid (Sigma, > 98%), and the concentration of Fe $^{3+}$ was determined by subtraction of the measured Fe $^{2+}$ concentration from the total dissolved iron.

Irradiation

Pulse radiolysis was performed using the 2.5 MeV Van de Graaff accelerator at Canadian Nuclear Laboratories. Pulses of electrons with energies of 2.25 MeV and pulse lengths of 0.5, 1, and 2 µs supplied doses of up to 10, 20, and 35 Gy per pulse respectively, allowing for the concentration of water radiolysis products to be varied to ensure pseudo-first-order kinetics were observed at all iron concentrations studied. The analysing light source was an Edinburgh Instruments Xe900 750 W xenon arc flash lamp. The optical system used a combination of a Bausch and Lomb monochromator with a Hamamatsu R166 photomultiplier and a Teledyne Lecroy Wavejet 354 oscilloscope. The absorbance of light at 304 nm was monitored over the duration of the reaction in order to follow the buildup of FeOH²⁺, the product of R2. Reaction rate coefficients are based on three replicates at each temperature, iron concentration, and pulse width.

Dosimetry was performed using the well-established thiocyanate system, using a value for Gε of 2.59 x 10⁻⁴ m² J⁻¹ at 475 nm¹⁶. An air saturated solution of 0.01 M potassium thiocyanate (99%) was used for dosimetry. A charge counting ring, which measures the current at the inlet to the irradiation vessel was calibrated against the chemical dosimetry. The counting ring collects electrons at the edge of the beam at the inlet to the irradiation vessel and a Red Nun RN-8111 current integrator is used to provide a digital signal to an Ortec 974 counter. The output of the counter has been demonstrated to be proportional to the beam intensity, and therefore dose. The dose per "count" recorded during dosimetry was used in conjunction with the output from the counter to determine the dose for each individual pulse when irradiating iron solutions. The solution was supplied to the reaction cell by a 50 mL glass syringe held in position inside an autoclave capable of operation at temperatures and pressures up to 300 °C and 10.3 MPa (1500 psi). The optical cell was heated using a copper heating block controlled using an Automation Direct temperature controller, and monitored using type K thermocouples. Optical quartz windows on the sides of the cell allow for the light from the arc flash lamp to pass through the solution perpendicular to the direction of the electron pulse. The solution in the reaction cell was refreshed after each pulse by draining the cell and allowing the solution in the syringe to replace the irradiated volume. At least 3 rinses of the cell were performed between pulses. The reservoir syringe was outside the heated area of the autoclave and shielded from secondary X-rays to prevent thermal or radiolytic changes occurring in the stock solution.

Examples of traces recorded at each temperature are presented in Figure 1.

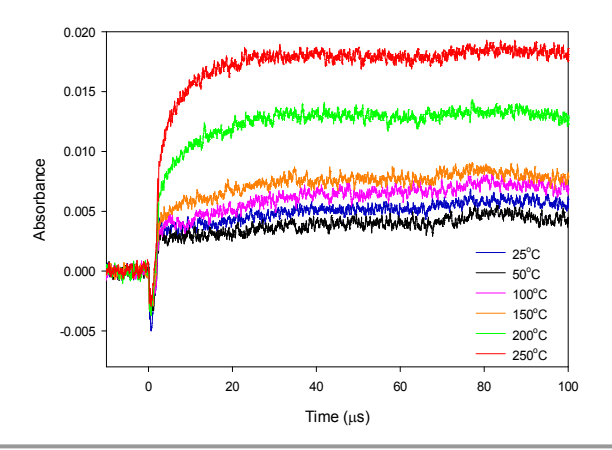


Figure 1: Kinetic traces recorded at 304 nm following 2 μs electron pulses of 1 x 10 4 M FeSO $_4$ solution at 25-250 $^\circ C.$

Observed rate constants were calculated from first order fits of the build-up of the reaction product from 3 replicates of each pulse width at each concentration of ferrous ions. Values for the rate constants and errors at each temperature were calculated from linear regression plots of ferrous ion concentration vs. observed rate constant. Activation energies were calculated from linearised Arrhenius plots of ln(k) vs. 1000/T (K^{-1}). Activation entropy and enthalpy, and the errors for each value were calculated from linear regression Eyring plots of lnk/T vs. 1000/T (K^{-1}).

Results

Temperature Dependence

The room temperature rate constant for R2 in light water was determined as (2.7 \pm 0.2) x 10 8 M $^{-1}$ s $^{-1}$, which is in good agreement with the values reported by Jayson *et. al.* and Stuglik and Zagorsky within the experimental error in this work and reported values from the authors (Table 1).

Table 1: Comparison of room temperature rate constants for the reaction of ferrous ions with *OH radicals measured by different research groups. †error calculated from figure. ‡no error or raw data available.

Reference	k (10 ⁸ M ⁻¹ s ⁻¹)
Christensen and Sehested ⁶ (1981) [†]	4.3 ± 0.6
Jayson <i>et. al.</i> ⁷ (1972)	2.3 ± 0.2
Stuglik and Zagorsky8 (1981)	3.2 ± 0.4
Zehavi and Rabani ⁹ (1971) [‡]	3.58
This work (2023)	2.7 ± 0.2

The measured room temperature rate constant is not close to the values of Christensen and Sehested, or Zehavi and Rabani, though neither of these papers report any error. The Christensen and Sehested paper includes individual data points that can be used to estimate the error at 6 x 10^7 M $^{-1}$ s $^{-1}$, but

includes few experimental details, making it difficult to comment on the source of the discrepancy.

Measuring values for the rate constant (k) across a range of temperatures allows for calculation of the activation energy (E_a) using the Arrhenius equation (eq 1), where A is the pre-exponential factor, R is the gas constant, and T is absolute temperature.

$$k = Ae^{\frac{-E_a}{RT}} (eq 1)$$

The measured rate constants from this work are shown as a function of temperature in Figure 2, in which there are two distinct regions, referred to as the low temperature (< 150 °C) and high temperature (> 150 °C) regions. The measured rate constant at 300 °C was lower than expected, and exhibited much greater uncertainty than other values. At 300 °C an orange precipitate was observed, indicating loss of iron from solution.

The low rate constant and high uncertainty at 300 $^{\circ}$ C are attributed to the precipitation of iron from solution leading to a lower effective rate constant. The orange precipitate was not observed at 250 $^{\circ}$ C.

The activation energies were calculated separately for each region, and data collected at 300 °C were omitted from calculation of the high temperature region activation energy. The activation energy in the low temperature region is close to zero, in the high temperature region the activation energy is $45.8 \pm 3.0 \text{ kJ mol}^{-1}$, which is similar to the value of $43.88 \text{ kJ mol}^{-1}$ for water exchange¹² in the inner hydration sphere for $[\text{Fe}(\text{H}_2\text{O})_6]^{2+}$.

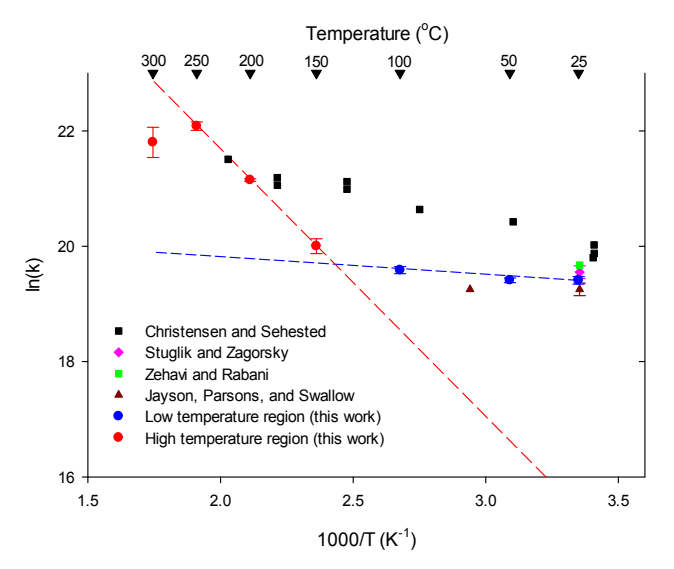


Figure 2: Arrhenius plot of experimentally determined rate constants across the temperature range $25-300\,^{\circ}\text{C}$ for the reaction of Fe^{2*} with 'OH radicals. Linear fits are extrapolated across the entire temperature range for each region. Literature data are included for comparison.

The inflection in the Arrhenius plot at 150 °C suggests a change in the dominant reaction mechanism. Although at low temperature one reaction mechanism is entirely dominant it is possible for the rate of a mechanism with a high activation energy to become competitive as the temperature increases.

Because the activation energy in the high temperature region is similar to the activation energy for the water exchange process in $[Fe(H_2O)_6]^{2+}$, it is suggested that the reaction proceeds via a dissociative ligand interchange mechanism, in which the rate limiting step is the loss of a water molecule from the inner hydration sphere. Dissociative ligand interchange (I_d) proceeds through the formation of a pre-encounter complex, in which the incoming ligand enters the outer hydration sphere with equilibrium constant K_{os} (R6).

$$M(H_2O)_6 + X \xrightarrow{K_{0s}} [H_2O - M(H_2O)_5 - X]$$

$$[H_2O - M(H_2O)_5 - X] \xrightarrow{k_{-H_2O}} M(H_2O)_5 X + H_2O$$
(R6)

Once the encounter complex is formed the incoming ligand competes with water molecules in the outer hydration sphere to replace it, a process that is limited by the rate of loss of the water ligand $(k_{\text{H}_2}\text{O})$. The overall rate of the dissociative interchange reaction (k_{Id}) reaction is proportional to K_{OS} and the rate of water loss¹⁷ (eq 2).

$$k_{\rm Id} \approx K_{\rm os} \times k_{\rm -H_2O}$$
 (eq 2)

It is possible to predict the rate of a dissociative interchange reaction between Fe²⁺ and *OH using the Eigen-Fuoss equation for reactants with no electrostatic interaction (eq 3) to predict the equilibrium constant for the formation of a pre-encounter complex, where a is the distance of closest approach (5.4 Å based on the radii of the two reactants)^{18,19} and N is Avogadro's number.

$$K_{\rm os} = \frac{4\pi N a^3}{3000}$$
 (eq 3)

For an uncharged reactant, K_{os} depends only on the radii of the reactants. The estimated rates of the dissociative ligand interchange reaction (k_{ld}) across the temperature range studied are summarised alongside the experimental data in Table 2.

Table 2: Comparison of observed rate constants ($k_{\rm obs}$) with predicted values based on a dissociative ligand interchange ($l_{\rm d}$) mechanism in the temperature range 25 – 250 °C. Uncertainties are calculated based on least squares regression plots of 3 concentrations and 3 pulse widths at each temperature.

T (°C)	Measured $k_{\rm obs}$ (10 ⁸ M ⁻¹ s ⁻¹)	Predicted k_{ld} (10 ⁸ M ⁻¹ s ⁻¹)	$k_{\rm obs}/k_{\rm Id}$
25	2.69 ± 0.18	0.02	153.50
50	2.69 ± 0.11	0.07	38.91
100	3.21 ± 0.20	0.62	5.19
150	4.86 ± 0.63	3.29	1.48
200	15.30 ± 0.33	12.31	1.24
250	38.90 ± 2.83	35.77	1.09

The measured rate of reaction becomes increasingly similar to the predicted rate of a dissociative ligand interchange reaction with increasing temperature. Although the low temperature hydrogen abstraction mechanism is initially faster than the dissociative mechanism, it has a much lower activation energy, allowing the I_{d} mechanism to become dominant at higher temperatures.

At temperatures < 150°C, there is no apparent change in the rate of the hydrogen abstraction reaction. This suggests either that the reaction is essentially barrierless or that the activation energy of the low temperature mechanism is negative. In the case of a barrierless reaction, the rate of reaction would be expected to be limited only by the rate of diffusion of the reactants, and to exhibit the same activation energy as diffusion. At room temperature the measured rate is 2 orders of magnitude slower than water diffusion. In order to determine whether the reaction becomes diffusion controlled at high temperature the rate of a diffusion limited reaction between Fe²⁺ and *OH radicals was estimated. The Smoluchowski equation²⁰ (eq 4), was applied in which k_{diff} is the rate constant of a diffusion-controlled reaction (M-1 s-1), D is the sum of the diffusion coefficients of the reactants (m^2 s⁻¹), and a is the distance of closest approach (m). Electrostatic terms are not included as only one of the reactants is charged.

$$k_{\rm diff} = 4\pi Da \qquad (eq 4)$$

The calculated values of $k_{\rm diff}$ are up to 2 orders of magnitude higher than the values of $k_{\rm obs}$ across the entire temperature range. This suggests that neither reaction mechanism can be considered diffusion limited.

Assuming that the hydrogen abstraction and ligand interchange mechanisms occur simultaneously in kinetic competition, the measured rate constant will be the sum of the rates of the individual mechanisms (eq 5).

$$k_{\rm obs} = k_{\rm I_d} + k_{\rm H_{abs}} \tag{eq 5}$$

The rate of the hydrogen abstraction reaction ($k_{\rm H_{abs}}$) was calculated based on the estimated value for the I_d reaction, and the measured overall rate constant. The reaction exhibits a negative activation energy of -0.36 kJ mol⁻¹. Arrhenius parameters for the two reaction mechanisms are summarised in Table 3.

Table 3: Calculated activation energies and pre-exponential factors for each mechanism involved in the reaction of OH with ferrous ions in the temperature range 25-300°C

Mechanism	E _a (kJ mol ⁻¹)	A (M ⁻¹ s ⁻¹)
HAT	-0.36 ± 0.11	2.3 ± 1.04 x 10 ⁸
ld	43.4 ± 0.40	$7.2 \pm 0.1 \times 10^{13}$

Negative activation energies have been observed before in oxidation reactions of Fe(II) complexes 21,22 , including $[\text{Fe}(\text{H}_2\text{O})_6]^{2^+}$. In all cases, the mechanism was hydrogen atom transfer (HAT), with the negative activation energy attributed to the large negative entropy change resulting from a decrease in the available vibrational modes in the transition state 23,24 . It is possible that a similar entropy change is present alongside the negative activation energy observed in the low temperature region of the oxidation of Fe $^{2^+}$ by *OH.

The empirical Arrhenius equation simplifies transition state theory and does not include provision for the effect of entropy on formation of the transition state. In order to properly

account for the properties of the transition state it is more appropriate to consider the Eyring equation (eq 6) which describes the entropy and enthalpy change required to reach the transition state prior to the formation of products.

$$k = \frac{k_B T}{h} e^{\frac{\Delta S^{\mp}}{R}} e^{\frac{-\Delta H^{\mp}}{RT}}$$
 (eq 6)

where $k_{\rm B}$ is the Boltzmann constant, T the absolute temperature, h Planck's constant, $\Delta {\rm H}^{\ddagger}$ the activation enthalpy, $\Delta {\rm S}^{\ddagger}$ the activation entropy, and R the gas constant. The predicted rate constants for the hydrogen abstraction mechanism across the temperature range are presented in an Eyring plot in Figure 3.

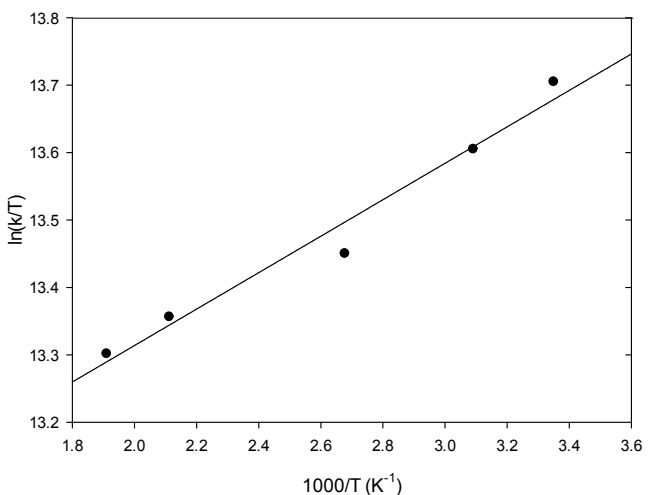


Figure 3: Eyring plot for the calculated rates of the hydrogen abstraction mechanism based on the measured rates of reaction and the calculated rate of the la reaction.

Eyring analysis of the kinetic data allows for calculation of ΔS^{\ddagger} and ΔH^{\ddagger} for each reaction mechanism. These thermodynamic properties are presented in Table 4.

Table 4: Calculated activation parameters for the reaction of ${}^{\bullet}OH$ radicals with ferrous ions in the temperature range 25-300 ${}^{\circ}C$

Mechanism	ΔS^{\ddagger}	ΔH^{\ddagger}
	JK ⁻¹ mol ⁻¹	kJ mol ⁻¹
HAT	-91.4 ± 7.1	-2.5 ± 0.2
DAT	-118.2 ± 7.7	-8.17 ± 3.2
I_d	11.4 ± 0.37	30.8 ± 3.7

The HAT reaction involves the formation of a transition state in which the rotation of the coordinated water molecules becomes stiffer due to the introduction of the incoming ligand, resulting in a significant decrease in the entropy of the transition state. The large decrease in entropy leads to an entropy-enthalpy compensation, which accounts for the relatively low pre-exponential factor, and the near-zero activation energy. The implication of the large entropy change is that the reaction may only proceed when coordinated water molecules are in specific orientations.

Kinetic Isotope Effect

In order to further differentiate the two reaction mechanisms, the experiments were repeated in heavy water. The kinetic

isotope effect (KIE) is the ratio of the rate constants in the two environments (eq 7), where $k_{\rm H}$ is the rate constant in light water, and $k_{\rm D}$ is the rate constant in heavy water.

$$KIE = k_{\rm H}/k_{\rm D} \tag{eq 7}$$

Because HAT involves transfer of a hydrogen atom, the reaction should exhibit a KIE in heavy water. The I_d mechanism, however, involves transfer of a water molecule, with only Fe-O bonds being broken and formed, so it should not exhibit any KIE in heavy water.

A comparison of the measured rate constants in light and heavy water is shown in Figure 4 alongside predicted rates based on eq 5 for light and heavy water. The predicted values fit well to the measured rate constants and illustrate the switchover in mechanism as the difference between measured rate constants in light and heavy water decreases with increasing temperature. The same issue with precipitation was encountered at temperatures > 200 °C in heavy water, resulting in a decrease in the observed rate constant due to lower concentrations of Fe $^{2+}$ in solution. The onset temperature for precipitation was lower than observed in light water. It is suggested that the observed decrease in the rate is the result of lower solubility of the iron salt in heavy water in comparison with light water.

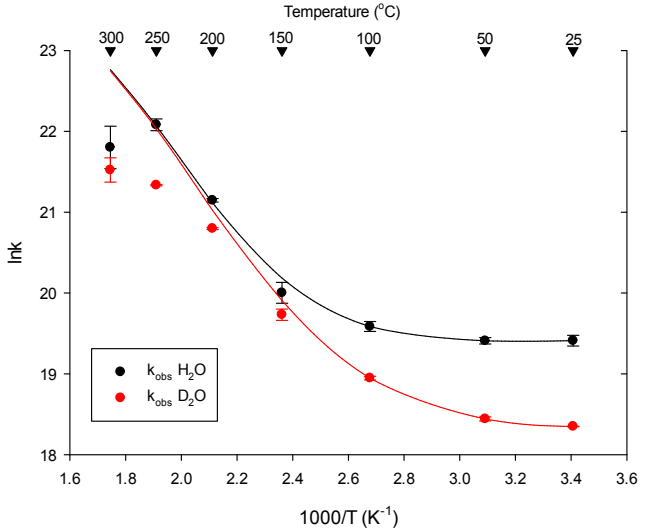


Figure 4: Comparison of measured rate constants in light water ($k_{\rm h}$) and heavy water ($k_{\rm o}$) in the temperature range 25 – 300 °C. Lines represent the predicted rate constants based on Arrhenius parameters and the kinetic isotope effect.

The convergence of the light and heavy water rate constants as temperature increases indicates a change in mechanism from hydrogen transfer to a mechanism that does not directly involve a hydrogen atom. This data supports the existence of a mechanistic switchover from HAT to dissociative ligand transfer. The DAT reaction does exhibit a positive activation energy, suggesting that the rates of the two processes would eventually converge. The KIE only decreases to 1.9 by a temperature of 300°C, indicating that the difference in activation enthalpies alone is not sufficient to account for the convergence of rate constants. This further supports the existence of a mechanistic switchover at higher temperatures.

The kinetic isotope effect in the low temperature region was originally attributed to differences in the energy of solvation in H_2O and D_2O^7 . It is proposed that the observed KIE is actually the result of the difference between the zero point energy of the hydrogen and deuterium forms of the transition state (ΔZPE_{TS}) and the ground state (ΔZPE_{GS}) of the products and reactants. A kinetic isotope effect is observed when ΔZPE_{TS} is significantly smaller than ΔZPE_{GS} due to the change in the relative energy required to overcome the activation energy barrier. When the activation enthalpy is small the transition state is a mid-point in the reaction coordinate between the reactants and products, meaning that the H/D atom is shared between the two molecules involved, the vibrational energy of the bonds in the transition state is nearly independent of the mass of the H/D atom. The result of such a transition state is a large difference between ΔZPE_{TS} and ΔZPE_{GS} , resulting in a large KIE²⁵. The observed KIE and the evidence of entropy-enthalpy compensation effects both support the formation of a transition state in which the hydrogen atom is shared equally between the coordinated water molecule and the *OH radical.

Conclusions

The reaction of the hydrated Fe²⁺ ion $[Fe(H_2O)_6]^{2+}$ with the hydroxyl radical has a non-Arrhenius temperature dependence. Between 25 – 150 °C the reaction proceeds via hydrogen atom transfer, while at temperatures > 150 °C, the dominant reaction is dissociative ligand interchange. The HAT reaction has a slight negative activation energy of -0.36 kJ mol⁻¹ as a result of a strongly negative activation entropy resulting from the loss of vibrational modes on formation of the transition state. The HAT reaction proceeds via an intermediate in which the proton is shared between the radical and the water ligand, resulting in a significant KIE and entropy-enthalpy compensation, which accounts for the near zero activation energy.

Dissociative ligand interchange is initially too slow to compete with HAT at room temperature, but the high activation energy of the rate limiting process of water exchange¹⁰ (43.88 kJ mol⁻¹) allows dissociation to become competitive with the rate of HAT at higher temperatures. At temperatures > 150 °C dissociative ligand interchange is the dominant reaction.

Kinetic isotope effect analysis shows a change in the nature of bonds formed and broken as temperature increases, with hydrogen atoms becoming decreasingly involved in the process. This supports a move from HAT to an I_d reaction mechanism.

Conflicts of interest

There are no conflicts to declare.

Acknowledgements

The authors thank Patrick Gicala for performing pulse radiolysis experiments in heavy water.

This study was funded by Atomic Energy of Canada Limited under the auspices of the Federal Nuclear Science and

Technology Program. Dr. Jacy Conrad is supported through the INL Laboratory Research & Development (LDRD) Program under DOE Idaho Operations Office Contract DE-AC07-05ID14517. The research was conducted at Canadian Nuclear Laboratories.

References

- G.V. Buxton, R.M. Sellers, Coord. Chem. Rev., 1977, 22 (3), 195-274
- 2 F.H. Sweeton, C.F. Baes Jr., J. Chem. Thermodyn., 1970. 2(4), 479-500
- P.R. Tremaine, J.C. LeBlanc, J. Solution Chem. 1980. 4(6), 415-442
- 4 P. Yadav, R. T. Olsson and M. Jonsson, *Radiat. Phys. Chem.*, 2009, **78**, 939–944.
- 5 A.J. Elliot, D.M. Bartels, 2009, AECL 153-127160-450-001
- 6 Z. Stuglik, Z.P. Zagorsky, Radiat. Phys. Chem., 1981. 17, 229-233
- 7 D. Zehavi, J. Rabani, *J. Phys. Chem.,* 1971, **75**, 1738-1744
- G.G. Jayson, B.J. Parsons, A.J. Swallow, J. Chem. Soc. Faraday Trans., 1972, 1(68), 2053-2058
- H. Christensen, K. Sehested, *Radiat. Phys. Chem.* 1981., 18, 723-731
- 10 J.W.T Spinks, R.J. Woods, *An Introduction to Radiation Chemistry 3rd Edition,* John Wiley and Sons, Inc., New York USA, 1990
- 11 P.A. Yakabuskie, J.M. Joseph, P. Keech, G.A. Botton, D. Guzonas, J.C.Wren, Phys. Chem. Chem. Phys., 2011, 13, 7198-7206
- 12 Y. Ducommun, K.E. Newman, A.E. Merbach, *Inorg. Chem.*, 1980, **19**, 3696-3703
- 13 L. Kazmierczak, D. Swiatla-Wojcik, M. Wolszczak, *RSC Adv.* 2017, **7**, 8800-8807
- 14 K. Kanjana, B. Cortin, A. MacConnell, D. M. Bartels, *J. Phys. Chem. A.*, 2015, **119**, 11094-11104
- 15 N. Sutin, B.M. Gordon, J. Am. Chem. Soc., 1961, 83, 70-73
- 16 G.V. Buxton, C.R. Stuart, J. Chem. Soc. Faraday Trans. 1995 91 (2), 279-281
- 17 W.H. Casey, T.W. Swaddle, Rev. Geophys. 2003, 41(2), 1008-1027
- 18 A. Pabis, J. Szala-Bilnik, D. Swiatla-Wojcik, *Phys. Chem. Chem. Phys.*, 2011, **13**, 9458-94686
- 19 H. Ohtaki, T. Radnai, Chem. Rev., 1993, , 93, 1157-1204
- 20 E.F Caldin, Fast Reactions in Solution, John Wiley and Sons, Inc., New York USA, 1964
- 21 J.N. Braddock, T.J. Meyer, J. Am. Chem. Soc., 1973, 95(10), 3158-3162
- 22 J.L. Cramer, T.J Meyer, Inorg. Chem., 1974, 13, 1250-1252
- 23 E.A Mader, E.R. Davidson, J.M. Mayer, *J. Am. Chem. Soc.* 2007, **129**, 5153-5166
- 24 E.A. Mader, V.W. Manner, T.F. Markle, A. Wu., J.A. Franz, J.M. Mayer, J. Am. Chem. Soc., 2009, 131(12), 4335-4345
- 25 G.S. Hammond, J. Am. Chem. Soc., 1955, 77, 334-338